Acc. Chem. Res. **1999,** *32,* 397−406

Crystal Structures of Molecular Gold Nanocrystal Arrays

ROBERT L. WHETTEN,*
MARAT N. SHAFIGULLIN, JOSEPH T. KHOURY,
T. GREGORY SCHAAFF, IGOR VEZMAR,
MARCOS M. ALVAREZ, AND
ANGUS WILKINSON

Schools of Physics & Chemistry, Georgia Institute of Technology, Atlanta, Georgia 30332-0430

Received April 15, 1998

1. Molecular Crystals of Giant Metallic Compounds

In early 1995, several of us[1] were exploring the properties of the first size-purified forms of the giant aurothiol cluster compounds, denoted by c-Au:SR (Figure 1a).[2] We found that they reversibly condensed to form intensely colored solid films or powders of excellent quality (Figure 1b). Our characterization of the various samples placed their molecular weights in the 40 000−200 000 kDa range (equivalent to 200−1000 Au atoms), as determined mass-spectrometrically, and electron microscopy images (Figure 1a) suggested that each compound had a crystalline metal *core* in the corresponding 1.8−3.0 nm range.[3]

However, the greatest surprise came during an initial structural examination of the solid films and powders by X-ray diffraction (Figure 1c): In addition to the expected diffuse peaks arising from the planes of Au atoms *within* individual nanocrystal cores, we found for each sample a sequence of intense, sharp Bragg peaks in the small-angle region. These peaks arise from spacings between planes of the nanocrystals within a giant, three-dimensional (3D) superlattice: *a crystal of nanocrystals*, idealized in Figure 1d.[1]

The high degree of ordering implied by these results was unexpected. It was well-known that the giant metal cluster compounds (those with >∼40 metal atoms) isolated during the preceding decade showed only short-range order in the solid state.[4−6] By contrast, each size-purified sample of the aurothiol clusters showed intense diffraction, in some cases with peak widths limited only by diffractometer resolution. Subsequent measurements at the National Synchrotron Light Source established both the high crystallinity of the new materials and that the series adopted bcc (body-centered cubic) or near-bcc packing structures, a result that was soon confirmed by transmission electron microscopy on ultrathin crystals.[3]

Stimulated by these findings, Luedtke and Landman conducted a monumental theoretical investigation,[7] based on realistic models for all interactions, predicting that both bcc and lower-symmetry structures, such as that shown in Figure 1e, will form from Au nanocrystals with various R = *n*-alkyl adsorbates. Subsequently, various packing structures (fcc, bcc, hcp, and lower symmetry) have indeed been found for many other gold (and silver) nanocrystal materials prepared with various thio adsorbates. A key concept emerging from this theoretical and experimental work is the tendency toward organization, or bundling, of *n*-alkyl chains, so as to fill space uniformly and obtain a maximally dense packing.

In the meantime, interest in this particular class of "molecular nanostructures" has grown enormously, as it was established that (i) they could be isolated in highly purified and robust forms over a wide size range extending from the molecular (∼20 atoms, ∼0.8 nm) to beyond 3 nm core size,[8−11] (ii) they can be variously functionalized and integrated into a variety of molecular, surface, and solid-state structures,[12−16] (iii) their cores behave electrically as single nanoelectrodes, with discrete redox waves extending in a "Coulomb staircase" pattern,[17−19] (iv) their electronic and optical properties are intensely structured, showing the effects of conduction-level quantization of a metallic $Au^{(0)}$ core,[20−22] and (v) their electrical conduction is dominated by correlated single-electron tunneling (Blockade−Staircase phenomena).[15,23,24] Concurrently, much device interest has been directed toward ultrathin films (2D arrays or monolayers) and 1D chains of such "nanoparticles"; these technically and theoretically more difficult fields are dominated by the enhanced role of disorder (defects) in reduced dimensions, as compared to 3D molecular crystals.

In this Account, we describe (section 2) how the 3D crystal structures of molecular metal nanocrystals can be viewed as a packing problem. We review the road to isolating and characterizing this series of new aurothiol compounds as molecular substances (section 3). By showing exemplary results from the solid-state structural investigations (section 4), we arrive at a phase diagram,

Robert L. Whetten is a Professor of Chemical Physics at the Georgia Institute of Technology. After earning a Ph.D. in chemistry from Cornell University, and serving as a postdoctoral fellow at Exxon Research & Engineering, he joined the chemistry faculty at UCLA in 1985. He moved to Georgia Tech in 1993.

Marat N. Shafigullin is currently a doctoral candidate with the School of Physics at the Georgia Institute of Technology.

Joseph T. Khoury earned his Ph.D. in Chemistry from UCLA in 1999, and is presently a postdoctoral associate at the Rowland Institute of Science.

T. Gregory Schaaff earned his Ph.D. in chemistry from the Georgia Institute of Technology in 1998. He is currently a postdoctoral associate at Oak Ridge National Labs in the Chemical and Analytical Sciences Division.

Igor Vezmar earned his Ph.D. in physics from the Georgia Institute of Technology in 1998. Currently he works as a consultant with Trilogy Software, Inc. in Austin, TX.

Marcos M. Alvarez received his Ph.D. in chemistry from UCLA in 1996. He has been a postdoctoral fellow at the Jet Propulsion Lab and is employed as a chemical engineer by Los Angeles County.

Angus Wilkinson is a graduate of Oxford University, and has been an Assistant Professor of Chemistry at the Georgia Institute of Technology since 1993.

10.1021/ar970239t CCC: $18.00
Published on Web 05/18/1999

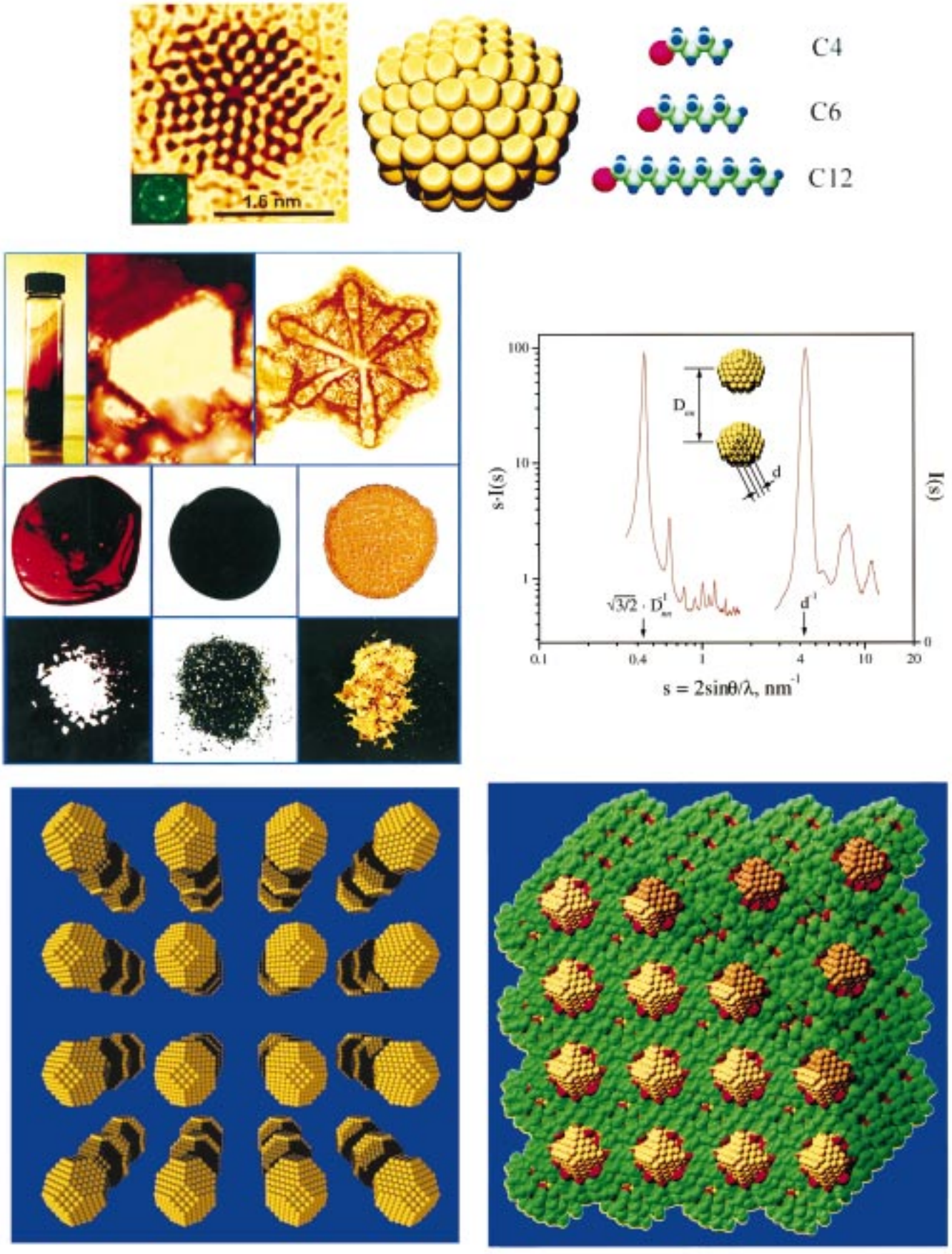

FIGURE 1. (a, top) Components of a giant aurothiol cluster (c-Au:SR) compound, drawn to scale, along with an electron micrograph confirming the core structure. The compound's core, at center, is represented in idealized form as consisting of 144 Au atoms (golden spheres). To it are

(Figure 1 caption continued) adsorbed a large number (∼56) of *n*-alkylthio groups, at right, where the red, green, and blue spheres represent, respectively, the sulfur, carbon, and hydrogen atoms; examples shown are butyl, hexyl, and dodecyl R groups. At left, an electron micrograph of a cluster assembly, on an amorphous-carbon support; only the Au atoms give sufficient contrast to be observed (refs 8−11). (b, middle left) Forms of aurothiol cluster compounds and related substances. In the lower row, the white noncrystalline solid is the polymeric compound (p-AuSR) employed as a precursor to the cluster compounds, the black fine powder is the crystalline cluster compound (29 kDa Au:SC6) representing the cluster phases c-Au:SR, the gold flakes at bottom right are the thermal decomposition products of a cluster-compound film, representing the extended-surface adsorbate phases s-Au:SR. In the middle row, thin and thick solid films of the cluster compounds are shown, along with a second photo of the latter after thermal decomposition to produce a very thin gold film (under reflected light) and an excess of desorbed disulfide (RSSR) on top. In the upper row, a concentrated solution of a cluster compound in toluene, illustrating the high concentration and optical density attainable, along with two of the crystal habits observed in larger crystals (40 and 65 μm, respectively), is shown. (c, middle right) X-ray diffraction from a powder of giant aurothiol clusters shows ordering on two distinct length scales. The scattering angle, $\theta \approx \sin(\theta)$, is plotted on a logarithmic scale, so that both regions can be viewed on an equal footing. (Right) The pattern at large angle reflects the internal ordering of the Au atoms within the cluster compound's nanocrystal core; the repeat distance between planes, $d = 0.23$ nm, is on the scale of the interatomic distance (0.29 nm). (Left) The spatial ordering of nanocrystals on a $D_{nn} \approx 3.0$ nm repeat distance is shown by the pattern at small angles, which is dominated by a series of intense Bragg peaks, with the intensity plotted on a logarithmic scale. The first seven peaks unambiguously demonstrate a bcc-type packing structure. (d, bottom left) Crystals of nanocrystals, an idealized illustration of a hierarchical structure, in which 586-atom truncated-octahedral Au nanocrystals (2.5 nm diameter) are arranged in a cubic (super)lattice. [The central columns of nanocrystals from a bcc-type structure have been removed for clarity of viewing.] Such a structure can explain the X-ray diffraction patterns observed. (e, bottom right) Theoretically predicted aurothiol compound structure, computed at room temperature, for 140-atom Au nanocrystals (assemblies of small gold spheres, 1.6 nm diameter, shown in cutaway view) with 62 *n*-butylthio groups adsorbed (red = sulfur atoms; green = methyl(ene) groups).

and present a geometrical interpretation. Several problems and opportunities exposed by this research are enumerated in the concluding section 5.

2. Crystal Lattice Structure as a Packing Problem

The spontaneous assembly of uniform-sized globular entities into ordered arrays is a universal phenomenon observed for objects with diameters spanning a vast range of length scales, from the atomic (10^{-8} cm), through the molecular and macromolecular (∼10^{-6} cm; proteins, synthetic low polymers, viruses, colloidal crystals), to the wavelength of visible light (∼10^{-5} cm; natural opals and synthetic spheres), and beyond, into the everyday packing of spherical objects (∼1 to 10^2 cm; balls, fruit). The associated concepts of sphere packing have had an influence in diverse fields ranging from pure geometrical analysis (cf. quasi-periodic structures) to architectural models or ideals.[25]

In material systems, the main factors determining the preferred crystal structure(s) of a given substance include not only any intrinsic structure (*shape*) of the object, but also its *softness*, encompassing both the compressibility−deformability of the individual entity and the nature and range of the interaction between entities. In the limit of extreme hardness and short-range ("contact") interactions, the close-packing structures—hexagonal (hcp) and cubic (fcc or ccp)—are optimal; these have the highest density, lattice symmetry, and coordination number. Crystallization of such solids is an entropically driven process, which has been thoroughly studied from both theoretical and experimental points of view.[26−28] However, even in the case of simple repulsive potentials (e.g., inverse power, or Yukawa type), the behavior of such systems is complex, and it is still not clear, for example, whether fcc structures are preferred over the random hexagonal close-packing (rhcp).[29,30] Naturally, in the case of softer entities, with longer-range and attractive potentials, lower symmetries and coordination numbers can be preferred.

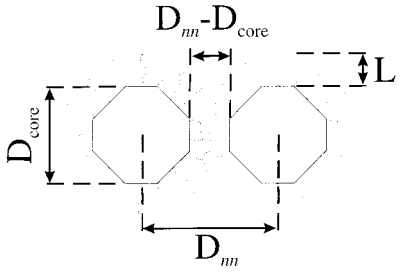

FIGURE 2. Schematic illustration of the core−corona structure and definition of parameters: L = thickness of the corona, equated to the fully extended (all-trans) chain length; D_{core} = the (equivalent) core diameter of the gold-nanocrystal core; D_{nn} = center-to-center distance between nearest neighbors in the solid state, a measure of the effective size of the assembly; $D_{nn} - D_{core}$ is a measure of the distance of closest approach of neighboring nanocrystals. The dimensionless parameter $\chi = 2L/D_{core}$ is also defined in terms of these quantities.

A large subset of "sphere-packing" phenomena involve systems in which a distinction can be made between a central *core*, that is dense and essentially nondeformable and incompressible, and a concentric-shell layer or *corona* that is comparatively diffuse and soft. Figure 2 illustrates this separation schematically, and defines the relevant dimensions (D) and spacings. For quantitative comparison, it is useful to define a dimensionless quantity

$$\chi = L/R = 2L/D_{core}$$

that expresses the thickness of the corona (L) relative to the radius (R) of the core.

Such a composite nature arises in many classes of matter. Perhaps the most familiar example is the set of chemical elements and the elemental solids they form. In an atom, the (ion) *core* has the noble-gas (filled-shell) configuration, and is spherical, relatively compact, and hardly deformed by bonding at the normal solid-state densities. The diffuse valence-electron cloud is primarily concentric to and outside the core, i.e., *coronal*, and may be strongly deformed in the elemental solid state. De-

pending on the diffuseness (χ) and specific deformability (valence) of the latter, the preferred structures may be close-packed (fcc, hcp), less densely packed (bcc; diamond, graphite, boron), or of a strongly broken symmetry (molecular forms for the halogens, chalcogens, N, and P). By analogy, this astonishing variety of structures arising from nominally spherical objects (atoms) can aid in understanding more complex systems.

Summarizing, the range of structures assumed by this newly discovered class of molecular-crystalline solids, comprised of metal nanocrystal cores compactly encapsulated by adsorbed chainlike thio groups, should be understood as an illuminating example of the properties of core−corona assemblies generally. The experimental origin and characteristics of these large molecular assemblies are presented next.

3. Giant Aurothiol Compounds as Molecular Nanostructures

In early summer 1994, we learned that Brust and Schiffrin in Liverpool had exploited phase-transfer catalysis to produce mixtures of large $Au_N(SR)_M$ clusters by a solution-phase reaction of aqueous Au salts and hydrophobic thiols (RSH) at room temperature.[2] After contacting Liverpool for further details, we immediately repeated their procedure, confirming their report that this method indeed produces quantitatively the highly stable clusters, with high solubility and other appealing properties. Comparing these with the laboriously aerosol-obtained clusters,[31] we found quite similar properties.[32] The solution-phase reactions[2] produced a mixture of clusters varying enormously in their core size, from ~1.5 nm or smaller to ~3 nm, or from ~70 to nearly 1000 Au atoms, necessitating extensive separations to avoid measurements that average over this distribution. Under heating or strongly reducing conditions, a polymer decomposition reaction (Figure 1b) was found to lead to the accumulation of the molecular forms

$$\text{p-AuSR} \rightarrow (1/N)\text{Au}_N(\text{SR})_M\ (= \text{c-Au}_1(\text{SR})_{1-x}) + (x/2)\text{RSSR}$$

or

$$\text{p-AuSR} + \text{Na} \rightarrow \text{c-Au}_1(\text{SR})_{1-x} + x\text{NaSR}$$

as a series of compounds tending asymptotically toward the surface s-Au:SR phases.

Space limitations preclude going beyond a simple enumeration of the (largely) nonstructural properties established for the various members of this series of new molecular metal nanostructure phases. Most striking is the emergence of a series of dominant compounds, spanning a wide range in metal core size (~20 to nearly 250 atoms).[8−11] Further, the choice of adsorbate group, further extended by the facile thiol-exchange reaction,[3,12,13] gives rise to a wide range of new phases. The assemblies appear in each case to consist of compact, crystalline cores, saturated at the surface by organic groups bound solely through the sulfur as expected given the special affinity for noble-metal surfaces. Some of the best evidence for this core-structural model is provided by the large-angle X-ray diffraction patterns, such as those shown in Figure 3.[33] The assemblies can be characterized by the usual methods employed for large molecules, and give results which tend to support the hypothesis that these are the finite analogues of the asymptotic extended-surface (SAM) phases.

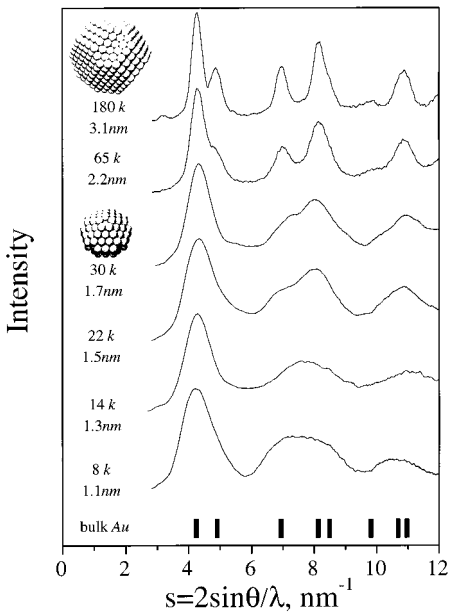

FIGURE 3. Evolution of the internal (core) structure with decreasing cluster mass (diameter) is reflected in the large-angle X-ray diffraction patterns. [The bars below indicate the locations of the bulk fcc-crystalline metal Bragg reflections.] Examples are selected to span the range from ~800 to ~40 atoms. The detailed line shapes in the pattern have been analyzed to exclude most of the structural models previously proposed for Au crystallites in the 1−2 nm diameter range (40−300 atoms).

4. Observed Packing Structures, Phase Diagram, and Interpretation

A. Prevalence of Crystals of Aurothiol Nanocrystal Compounds. Molecular crystals are found to form spontaneously from aurothiol compounds with *n*-alkyl chains as short as C_4 and as long as C_{18}, with core (nanocrystal) diameters from 1.4 nm ($N \approx 75$ atoms) to 3.2 nm (800 atoms) for Au, or with Ag to above 5 nm (3000 atoms). In this range, the number of adsorbates per metal atom (M/N) is estimated to range from ~0.6 to 0.3. The dimensionless corona-to-core ratio χ spans nearly a full order of magnitude, $\chi \approx 0.4-3$, centered about unity. When this full range was examined, a unified picture immediately emerged, as we now describe.

For each sample, the size parameters in Figure 2 are deduced from routine characterization. Typical sizing results, as obtained for a size series of Au:SC_6 compounds, are presented in Figure 4, which collects the principal peaks appearing in the mass spectrum and the small-angle region of the X-ray diffraction pattern. From the former, one calculates an effective core diameter D_{core}, using the bulk density (59 nm^{-3}) of crystalline Au. From the latter,

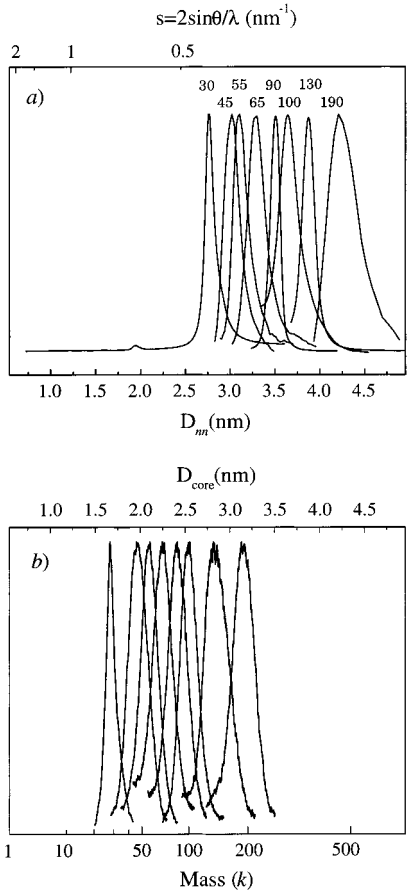

FIGURE 4. Determination of structural parameters (D_{nn}, D_{core}) for a range of R = C6 Au:SR cluster compound samples. (Top) The first peak in the small-angle diffraction pattern, used to obtain values for D_{nn} (see Figure 2). Values above each peak correspond to Au core masses in kilodaltons, as determined by mass spectrometry. (Bottom) The main peak in the laser-desorption mass spectra of the same compounds, used to obtain an estimate for D_{core}, assuming the density of bulk gold (as suggested by the invariance of peak positions in Figure 4).

one calculates a nearest-neighbor (center-to-center) distance, D_{nn}, using the complete indexing of the small-angle powder pattern. For the bcc and fcc lattices obtained with Au:SC_6, the conversion is $D_{nn} = (3/2)^{1/2}\ s^{-1}$. The dimensionless ratio χ is then calculated, $\chi = 2L/D_{core}$, using the length of the fully extended (all-trans) chain C_m ($L \approx (m + 1)0.12$ nm). Cross-comparison among nanocrystals with different adsorbate chains is possible because the core structure (Figure 3) is negligibly affected by the length of the adsorbate chain.

For solid-state structure measurements, highly purified samples are prepared as powders, thick films, thin films, or small single crystals. In the first case, homogeneous precipitation in solution is carried out by slow addition of a nonsolvent to a saturated solution. In the second, one dries drop-cast saturated solutions, in either air or vacuum, with or without heating. Very thin crystalline films or monocrystals are prepared on electron-microscopy supports (usually amorphous carbon films) by crystallization either in solution or directly on the support. The samples have been investigated in all these forms, by a combination of XRD (conventional and synchrotron sources) and

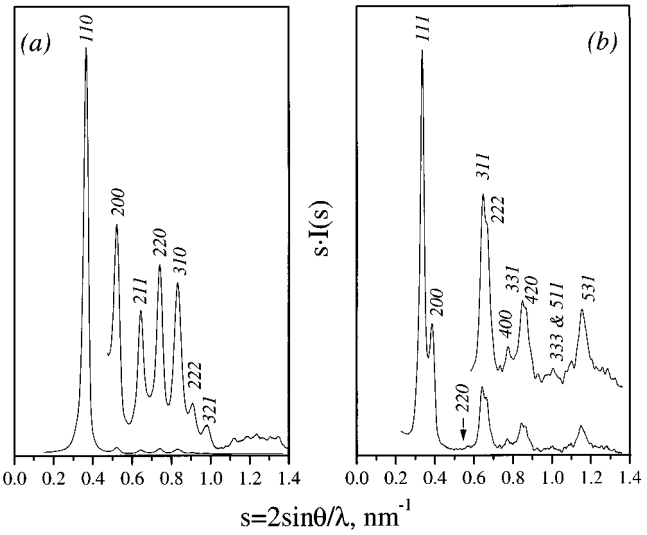

FIGURE 5. Distinct (fcc vs bcc) packing structures for different core sizes. The indexing of small-angle X-ray diffraction patterns for two exemplary samples. In (a), a 45 kDa Au:SC6 sample gives rise to a clear bcc pattern, as determined by the location of the first seven peaks. In (b), a 90 kDa Au:SC6 sample is indexed to an fcc structure. Accidental peak vanishings, such as the eighth peak in (a) and the 220 peak in (b), accurately reflect the size of the cluster's nanocrystal core.

high-resolution electron microscopy (HREM, SEM) and diffraction (ED). The synchrotron XRD results were obtained using a combination of reflection (near-grazing incidence) and transmission (near-normal incidence) on appropriate substrates (usually silicon wafers and thinned mica plates, respectively).

B. Structures Observed and a Phase Diagram. Typical XRD results, illustrative of the structures found in the moderate range of χ, are shown in Figures 5 and 6, with the deduced structural parameters gathered in Figure 7. Figure 5 shows XRD patterns for two powder samples, along with their unambiguous indexing to bcc and fcc lattices. The indexing precision is very high in either case, but the bcc lattices are better ordered. In the bcc structure, the presence of the seventh peak of the series is important, as it is one of the criteria that can be used to rule out the simple-cubic (sc) structure.

Detailed calculations of the intensity patterns, such as that shown in Figure 6, confirm that there is invariably *one* nanocrystal per lattice site. This permits a calculation of the *metal volume fraction* (see Figure 7c) from the core mass and the lattice constant. Intensity analyses also confirm that the core is largely globular, and are described in detail in a separate report.[34]

Nearly all the Au:SR samples of short or moderate chain length could be classified as bcc or fcc, but some show a lower symmetry, e.g., body-centered tetragonal (bct) with ~15% elongation along one axis, in which case a strong preferred orientation is observed in film samples. An example of apparent coexistence between bcc and fcc structures has also been observed. These exceptions do not prevent a clear classification of the structures as generally fcc or bcc, as indicated by the filled (unfilled) symbols in Figure 7.

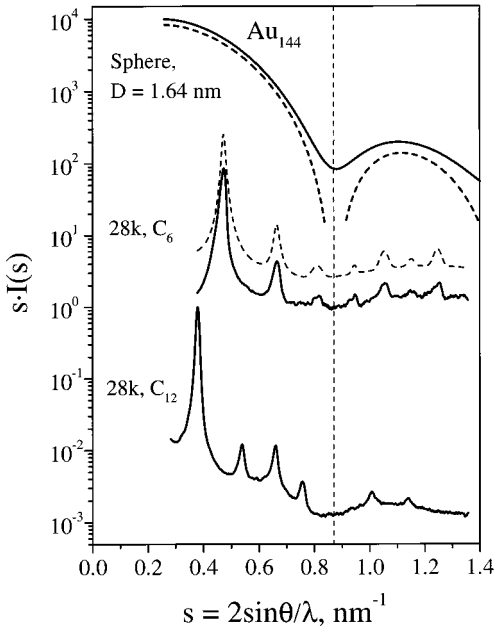

FIGURE 6. A single, globular core for each lattice site. The relative intensities in the small-angle X-ray diffraction pattern reflect the size and number of cores associated with each lattice site. At top, the calculated form factor for the 28 kDa Au-cluster core, modeled as a sphere of bulk density and mass-equivalent diameter (thick dashed line) and by the truncated-decahedral model (cf. Figure 1a). At the bottom and center, the experimental diffraction patterns, for samples with C12 and C6 chains. Also at center (dashed curve), the calculated intensity pattern using the C6-derived lattice constant, the sphere form factor, and a best-fit thermal factor. The vertical dashed line indicates the vanishing in the sphere's form factor, which appears as a minimum in the truncated-decahedron structure's form factor, accounting for the vanishing of the fifth peak in the C12 pattern, and relative peak intensities in the C6 pattern.

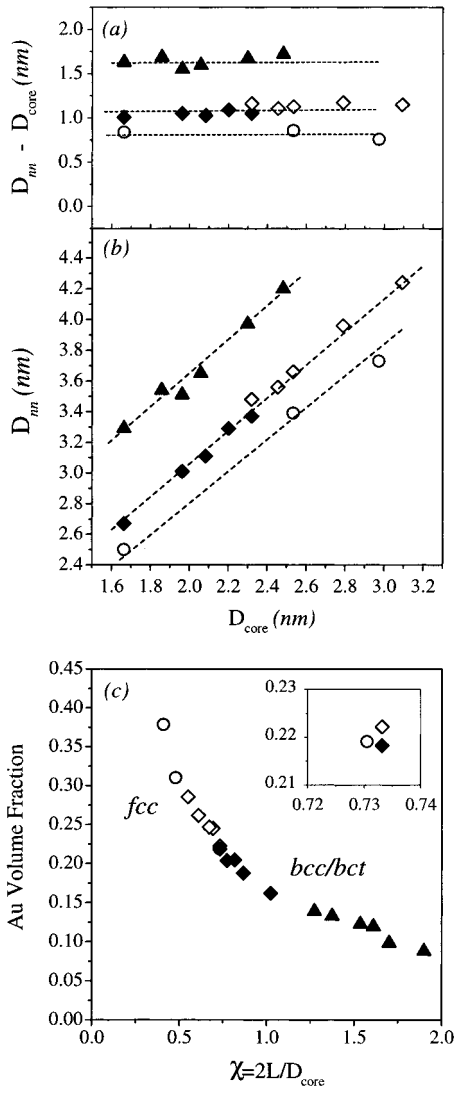

FIGURE 7. Collected structural parameters and phase diagram for the Au:S(*n*-alkyl) systems. [Please refer to Figure 2 for the definition of the parameters and to Figure 4 for an example of how they are determined.] The symbol code is the following: triangles = C12, diamonds = C6, circles = C4; filled symbols = bcc (or bct) structure observed, empty symbols = fcc structure observed. (a, b) The distance of closest approach observed with each of the various *n*-alkyl groups is nearly invariant to the Au-core diameter, a behavior also reflected in the straight-line variations in (b). (c) The computed core (Au) volume fraction of the various samples, plotted against the dimensionless corona-to-core ratio χ. The fcc and bcc/t regions of the diagram are indicated by unfilled (filled) symbols, with the boundary occurring at χ just above 0.70. The inset shows overlapping points in the vicinity of the (22% Au volume, $\chi = 0.73$) point.

The estimate for the distance of closest approach, $D_{nn} - D_{core}$ (cf. Figure 2), can be calculated, and is shown in Figure 7a. Its value is seen to be nearly constant for a given chain length, and is generally much less (usually about half) than expected of a bilayer of fully extended chains ($\sim 2L$ plus a van der Waals spacing). This implies a very high packing efficiency of the void space around the nanocrystal cores. Indeed, an accurate accounting of the density, using the measured composition of the compounds, indicates that the chain-packing densities are approximately equal to or somewhat higher than in the corresponding solid-crystalline (neat) alkane phases! This remarkable result was also predicted theoretically in ref 7, and places a strong constraint on the models that could describe the origin of these structures.

The diverse information can be simplified considerably by plotting against the dimensionless parameter χ (Figure 7c). The metal volume fraction is used as the other axis. Here the points fall along a common curve, with a pair of samples (showing both fcc and bcc characteristics) lying at a dividing point or boundary between fcc ($\chi < 0.72$) and bcc ($\chi > 0.75$) regions.

This picture can be extended to smaller values of χ (higher metal volume fraction) by observations on the larger Ag nanocrystals (4−6 nm diameter) passivated by C_{12} chains, which are conveniently observed as thin monocrystals (platelets) by HREM and ED. Two kinds of structures are predominantly observed in the work of refs 35 and 36. The first, observed with smaller Ag nanocrystals, are fcc, as shown by the ubiquitous appearance of images of small platelets in the 110 orientation. The second, observed with larger Ag nanocrystals, always take the hcp form with the basal plane oriented parallel to the support. In normal incidence one observes patterns that can be assigned uniquely to hcp only by comparison with simulated patterns. Unambiguous identification of the hcp

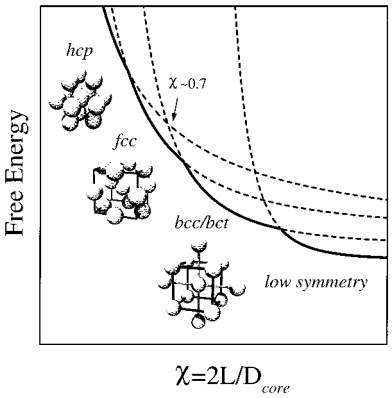

FIGURE 8. Hypothetical phase diagram for the Au:S(*n*-alkyl) family, represented in a free energy vs χ plot to indicate the regions of stable and metastable (not observed) phases. In the structural models, each gold sphere represents a nanocrystal (core), not a single Au atom; the bcc illustration includes four second-nearest neighbors (see the text). The hcp phases have been observed only in thin crystals of Ag:SC12 samples (refs 43 and 44). The lower-symmetry phases, observed, e.g., with C18, are usually observed only as films (not crystalline powders). The transition identified in Figure 7 is marked here for comparison.

structure, with an essentially ideal c/a ratio, requires a second observation at 45°. This latter structure has been investigated in great detail, because it forms over vast monocrystalline regions (many micrometers) with nearly uniform thickness; it is the subject of a report presented in ref 36. This evidence could be taken as supporting an fcc−hcp structural transition somewhere in the region near 50% volume fraction, or approximately two-thirds of the space filling.

At $\chi > 2$ (low metal volume fraction), results for smaller Au nanocrystals with long chains (C_{18}) cannot be ascribed to cubic or nearly cubic structures. A pattern of sharp and diffuse peaks could be evidence of a strongly uniaxial cell with good ordering in one dimension only. At present, we take this as evidence of a preference for lower symmetry structures.

C. Interpretation of the Phase Diagram. The variation of basic structural parameters (core size and coronal layer thickness) within a single class of molecular metal−nanocrystal systems with *n*-alkyl groups generates a number of distinct structure types in well-defined crystal lattices. These include hexagonal and two types of cubic structures, as well as lower-symmetry types (body-centered tetragonal and others). Such complexity from a single homologous series may appear bewildering. But the identification of a single determining geometrical parameter (χ), an intrinsic property of the individual molecular assembly, organizes this diversity, and suggests the highly schematic phase diagram (Figure 8) consistent with the results obtained to date. Moving from left to right, one imagines the high-symmetry, high-coordination number structures (hcp, fcc) becoming destabilized by the increasing "softness", as the monolayers become thicker in comparison to the hard-core dimensions, with respect to lower-symmetry, more "open" structures (bcc, bct), and then to noncubic structures.

This picture recalls other classes of materials systems in which softness of the coronal layer results in structures of (nominally) lower packing density, coordination number, and symmetry: structures of the elemental solids as organized conventionally on the periodic table of the elements, models of screened Coulombic (plasmas or ionic solutions) systems interacting via the repulsive Yukawa potential, and polymer-based micellar systems with dense cores.[27] The sequence hcp−fcc−bcc−(bct or lower) is not an unexpected one for real solids with both attractive and repulsive interactions, as can be seen by analogy to the first of these: hcp is favored, at least theoretically, for crystals of the rare gases (with no corona, $\chi = 0$), fcc and hcp dominate the elemental metals having contracted s-orbitals, bcc accounts for most of the other metals, and lower symmetry is found wherever small cores and large (many-electron) valence shells are present.

This line of reasoning says little about the organization of the chains in the molecular-nanocrystal arrays and offers no predictions concerning the values of χ at which one structure becomes destabilized by another. However, the experimental fact that the chain-packing density (in the bcc/bct structures) is comparable to that of crystalline alkanes at ambient pressure, combined with the discovery in simulations of strongly broken symmetry (bundling) in isolated and condensed forms of Au:SR passivated nanocrystals, inspires the idea that the transitions may be predicted geometrically in terms of the dimensions of the fully extended dense bundles that could assemble (at a given value of χ) and the optimal packing of such multibundled objects into lattices. Molecular dynamics computations show that van der Waals attractive interactions between surface groups belonging to nearest- and next-nearest-neighboring nanocrystal assemblies are the dominant contributors to the intercrystallite energy,[7] and maximally dense packing should naturally correspond to its minimization.

We have separately given this idea a quantitative expression, bounding the fcc−bcc transition in the range $0.4 < \chi < 1.0$. The qualitative reasoning is the following: First, in the limit of very short chains, χ tending to zero, the chains must assume the "brush" configuration, because it is the only one allowed for dense tethering on an effectively flat surface (large radius of curvature). Either hcp or fcc gives the maximum possible (12) contact interactions between brushes, assuming the core is not too far from spherical. Contact interactions between next-nearest neighbors are not possible in any of these lattices, so that filling of the void space by the chains is inefficient. hcp may be favored by the long-range intercore attractions, much as in rare-gas crystals. With increasing χ, there comes a point in any of the structures where second-nearest-neighbor contacts can form, assuming only that the chains can reorient away from the nearest-neighbor contacts and toward the second-nearest neighbors. The distance of closest approach between neighboring nanocrystals, which is rather invariant to core size, can be used, along with the fully extended chain length L and the core size D_{core}, to predict at what minimum value of χ such

contacts become possible, and at what value they will be optimal, for any given structure. For the bcc structure, the six second-nearest neighbors are centered at a distance only 15% greater than that of the nearest-neighbor centers (Figure 8), implying that filling space in those directions with six bundles will be effective at relatively small χ. Below ~0.4, there is no driving force for the bcc structure; somewhere above this value, as the chains from two bundles make better contact, the bcc structure may cross the fcc structure in stability, with 14 vs 12 contacts and better space-filling. Above ~1.0, bcc is destabilized with respect to other (lower-symmetry) structures.

In favoring this explanation, we have considered several others:

(i) A universal, entropically driven transition from close-packing (fcc) to the bcc structure is predicted to occur just below the solid−liquid transition.[37] We have searched for a solid−liquid transition and for an fcc-to-bcc transition with increasing temperature, but have found nothing at temperatures below those at which decomposition starts (~160 °C). An entropic explanation is diametrically opposed to the high chain densities observed here, and to the compact, ordered structures found in the extensive finite-temperature simulations incorporating realistic interactions.

(ii) A theory of the fcc−bcc transition for globular objects, interacting through repulsive radial potentials of varying softness (Yukawa form),[27] has been used by Gast and co-workers to account for the phase boundaries discovered in dense micellar solutions formed from diblock copolymers.[38] These systems have a manifestly core−coronal nature, with one block from each polymer contributing to the dense core and the second extending into the solvent. Despite the appeal of this picture, we doubt that an effective radial potential is decisive at the high densities of molecular nanocrystal solids. In the language of the tethered polymers, only the "brush" configuration is relevant. The "star" configuration, which may be natural in good solvents, is unstable with respect to bundling during the condensation process.

(iii) At another extreme, one could argue that the crystal structures are determined by the specific morphology (faceting) of the nanocrystal cores observed in high-resolution electron microscopy. This is a most interesting explanation, and we have searched for indications that it occurs in at least some cases. However, the effects of faceting should be greatest with short chains, whereas the opposite is observed.

The main strength of the research described in this Account lies in its exploration of the large range of relevant parameters. Other reports of three-dimensional organization of passivated nanocrystals typically described small (<1 μm) regions of a single sample that had undergone little if any size separation.[39,40] In the few cases where extended lattices have been observed and characterized in a statistically significant way, the range of structural parameters has been so small that only a single structure type is found, and these differ from one investigation to another, which could lead to the impression that each structure type is system-specific. Our results show that this clearly is *not* the case. In the semiconductor nanocrystal CdSe:OPR_3 solids described by Murray et al.,[41] only fcc packing structures are found with hcp characteristics intermixed; longer-range order is found only in one dimension, i.e., with oriented-film samples. The steric requirements of the PR_3 groups may also limit the organizational freedom of the adsorbate corona. Bentzon et al.[42] first reported long-range crystalline order in films prepared on electron-microscope grids; the structure type was determined indirectly, by comparison to simulations, as hcp. All the materials described above are of superior crystallinity, but initially only bcc lattices were found.

5. Challenges and Opportunities

From the systematics and interpretation in terms of space-filling bundles of adsorbate chains, several extensions and implications lie ahead: First, the action of applied pressure should be in the same sense as increasing χ, so that systems just below an ambient-pressure phase boundary (Figure 8) would show transitions to the higher-χ phase under pressure. Crystallization at temperatures far from the ambient might "freeze in" different configurations of adsorbed chain bundles, thereby shifting the phase boundaries to higher or lower χ. A large effect may be realized by employing branched, as opposed to straight, chain groups, which may prevent the kind of bundling proposed to explain the bcc phase. Expanded states might be prepared simply by cocrystallization with long-chain or globular molecules that can be incorporated in an ordered way into the voids. Finally, this investigation provides a good basis for the exploration of binary systems (alloys of passivated nanocrystals of distinct core and/or corona dimensions) that can exhibit additional interesting structures.[43]

The electronic and optical properties of these high-dielectric solids will be of interest, particularly for crystals grown from *charged* cluster cores with small HOMO−LUMO gaps, as might be grown electrochemically. For applications generally, it is widely held that the functionality of nanostructured materials requires that they are spatially organized in a well-controlled and -characterized manner. The findings described herein provide a firm phenomenological foundation in at least one broad area, that of spontaneously formed 3D arrays as molecular crystals.

We are particularly grateful to our colleagues (P. W. Stephens, S. A. Harfenist, Z. L. Wang, U. Landman, W. D. Luedtke, M. Jose-Yacaman, M. Hostetler, R. W. Murray, and S.-W. Chen) who have collaborated in aspects of the work described above, and to others who have provided preprints of their work prior to publication. This research has been supported by the National Science Foundation, the Office of Naval Research, the Packard Foundation, and the Georgia Tech Foundation.

References

(1) Whetten, R. L. In *The Chemical Physics of Fullerenes, 5 & 10 Years After*; Adreoni, W., Ed.; Kluwer: Dordrecht, The Netherlands, 1996; pp 475−490.

(2) Brust, M.; Walker, M.; Bethell, D.; Schiffrin, D. J.; Whyman, R. Synthesis of thiol-derivatised gold nanoparticles in a two-phase liquid−liquid system. *J. Chem. Soc., Chem. Commun.* **1994**, 801−802.
(3) Whetten, R. L.; Khoury, J. T.; Alvarez, M. M.; Murthy, S.; Vezmar, I.; Wang, Z. L.; Stephens, P. W.; Cleveland, C. L.; Luedtke, W. D.; Landman, U. Nanocrystal Gold Molecules. *Adv. Mater.* **1996**, *8*, 428−433.
(4) Bradley, J. S. In *Clusters and Colloids*; Schmid, G., Ed.; VCH: Weinheim, 1994.
(5) Schmid, G. Large clusters and colloids. Metals in the embryonic state. *Chem. Rev.* **1992**, *92*, 1709−1727.
(6) Vogel, W.; Rosner, B.; Tesche, B. Structural investigations of Au_{55} organometallic complexes by X-ray powder diffraction and transmission electron microscopy. *J. Phys. Chem.* **1993**, *97*, 11611−11616.
(7) Luedtke, W. D.; Landman, U. Structure, Dynamics, and Thermodynamics of Passivated Gold Nanocrystallites and Their Assemblies. *J. Phys. Chem.* **1996**, *100*, 13323−13329.
(8) Schaaff, T. G.; Shafigullin, M. N.; Khoury, J. T.; Vezmar, I.; Whetten, R. L.; Cullen, W. G.; First, P. N.; Gutierrez, C.; Ascensio, J.; Jose-Yacaman, M. J. Isolation of smaller nanocrystal Au molecules: robust quantum size effects in optical spectra. *J. Phys. Chem.* **1997**, *B101*, 7885−7891.
(9) Schaaff, T. G.; Knight, G.; Shafigullin, M. N.; Borkman, R. F.; Whetten, R. L. Isolation and Selected Properties of a 10.4 kDa Gold: Glutathione Cluster Compound. *J. Phys. Chem.* **1998**, *B102*, 10643−10646.
(10) Schaaff, T. G. Dissertation, Georgia Institute of Technology, 1998.
(11) Alvarez, M. M.; Khoury, J. T.; Schaaff, T. G.; Shafigullin, M. N.; Vezmar, I.; Whetten, R. L. Critical sizes in the growth of Au clusters. *Chem. Phys. Lett.* **1997**, *266*, 91−98.
(12) Hostetler, M. J.; Green, S. J.; Stokes, J. J.; Murray, R. W. Monolayers in Three Dimensions: Synthesis and Electrochemistry of ω-Functionalized Alkanethiolate-Stabilized Gold Cluster Compounds. *J. Am. Chem. Soc.* **1996**, *118*, 4212−4213.
(13) Templeton, A. C.; Hostetler, M. J.; Craft, C. T.; Murray, R. W. Reactivity of Monolayer-Protected Gold Cluster Molecules: Steric Effects. *J. Am. Chem. Soc.* **1998**, *120*, 1906−1911.
(14) Leff, D. V.; Ohara, P. C.; Heath, J. R.; Gelbart, W. M. Thermodynamic control of gold nanocrystal size: experiment and theory. *J. Phys. Chem.* **1995**, *99*, 7036−7041.
(15) Andres, R. P.; Bielefeld, J. D.; Henderson, J. I.; Janes, D. B.; Kolagunta, V. R.; Kubiak, C. P.; Mahoney, W.; Osifchin, R. G. Self-assembly of a two-dimensional superlattice of molecularly linked metal clusters. *Science* **1996**, *273*, 1690−1693.
(16) Hostetler, M. J.; Murray, R. W. Colloids and self-assembled monolayers. *Curr. Opin. Colloid Interface Sci.* **1997**, *2*, 42−50.
(17) Green, S. J.; Stokes, J. J.; Hostetler, M. J.; Pietron, J.; Murray, R. W. Three-dimensional monolayers: nanometer-sized electrodes of alkanethiolate-stabilized gold cluster molecules. *J. Phys. Chem.* **1997**, *B101*, 2663−2668.
(18) Ingram, R. S.; Hostetler, M. J.; Murray, R. W.; Schaaff, T. G.; Khoury, J. T.; Whetten, R. L.; Bigioni, T. P.; Guthrie, D. K.; First, P. N. 28 kDa Alkanethiolate-protected Au clusters give analogous solution electrochemistry and STM coulomb staircases. *J. Am. Chem. Soc.* **1997**, *119*, 9279−9280.
(19) Chen, S.; Ingram, R. S.; Hostetler, M. J.; Pietron, J. J.; Murray, R. W.; Schaaff, T. G.; Khoury, J. T.; Alvarez, M. M.; Whetten, R. L. Gold nanoelectrodes of varied size: Transition to molecule-like charging. *Science* **1998**, *280*, 2098−2101.
(20) Alvarez, M. M.; Khoury, J. T.; Schaaff, T. G.; Shafigullin, M. N.; Vezmar, I.; Whetten, R. L. Optical absorption spectra of nanocrystal gold molecules. *J. Phys. Chem.* **1997**, *B101*, 3706−3712.
(21) Collier, C. P.; Saykally, R. J.; Shiang, J. J.; Henricks, S. E.; Heath, J. R. Reversible tuning of silver quantum dot monolayers through metal−insulator transition. *Science* **1998**, *277*, 1978−1981.
(22) Khoury, J. T.; Alvarez, M. M.; Schaaff, T. G.; Shafigullin, M. N.; Whetten, R. L. Discrete transitions in the optical dielectric response of giant gold cluster compounds. Submitted for publication.
(23) Terrill, R. H.; Postlethwaite, T. A.; Chen, C.-h.; Poon, C.-D.; Terzis, A.; Chen, A.; Hutchison, J. E.; Clark, M. R.; Wignall, G.; Londono, J. D.; Superfine, R.; Falvo, M., Jr.; C. S. J.; Samulski, E. T.; Murray, R. W. Monolayers in three dimensions: NMR, SAXS, thermal, and electron hopping studies of alkanethiol stabilized gold clusters. *J. Am. Chem. Soc.* **1995**, *117*, 12537−12548.
(24) Brust, M.; Bethell, D.; Schiffrin, D.; Kiely, C. L. Novel gold-dithiol nano-networks with nonmetallic electronic properties. *Adv. Mater.* **1995**, *7*, 795−797.
(25) Williams, R. *The Geometrical Foundation of Natural Structure*; Dover: New York, 1979.
(26) Gast, A. P.; Russel, W. B. Simple Ordering in Complex Fluids. *Phys. Today* **1998**, *51*, 24−30.
(27) Robbins, M. O.; Kremer, K.; Grest, G. S. Phase diagram and dynamics of Yukawa systems. *J. Chem. Phys.* **1988**, *88*, 3286−3312.
(28) Russel, W. B.; Chaikin, P. M.; Zhu, J.; Meyer, W. V.; Rogers, R. Dendritic Growth of Hard Sphere Crystals. *Langmuir* **1997**, *13*, 3871−3881.
(29) Pusey, P. N.; Megen, W. v.; Bartlett, P.; Ackerson, B. J.; Rarity, J. G.; Underwood, S. M. Structure of Crystals of Hard Colloidal Spheres. *Phys. Rev. Lett.* **1989**, *63*, 2753−2756.
(30) Zhu, J.; Li, M.; Rogers, R.; Meyer, W.; Otteweill, R. H.; Crew, S.-S. S.; Russel, W. B.; Chaikin, P. M. Crystallization of hard-sphere colloids in microgravity. *Nature* **1997**, *387*, 883−885.
(31) Alvarez, M. M. Dissertation, University of California, 1996.
(32) This comparison, along with initial separations, was reported at the ISSPIC-7 meeting in Kobe, Japan, September 1994.
(33) Cleveland, C. L.; Landman, U.; Schaaff, T. G.; Shafigullin, M. N.; Stephens, P. W.; Whetten, R. L. Structural evolution of smaller gold nanocrystals: The truncated decahedral motif. *Phys. Rev. Lett.* **1997**, *79*, 1873−1876.
(34) Shafigullin, M. N. Manuscript in preparation.
(35) Harfenist, S.; Wang, Z. L.; Alvarez, M. M.; Vezmar, I.; Whetten, R. L. Highly oriented moleculat Ag nanocrystal arrays. *J. Phys. Chem.* **1996**, *100*, 13904−13910.
(36) Harfenist, S. A.; Wang, Z. L.; Whetten, R. L.; Vezmar, I.; Alvarez, M. M. Three-dimensional hexagonal close-packed superlattice of passivated Ag Nanocrystals. *Adv. Mater.* **1997**, *9*, 817−822.
(37) Chaikin, P. M.; Lubensky, T. C. *Principles of Condensed Matter Physics*; Cambridge University Press: Cambridge, New York, 1995; pp 188−192.
(38) McConnell, G. A.; Gast, A. P.; Huang, J. S.; Smith, S. D. Disorder−order transitions in soft sphere polymer micelles. *Phys. Rev. Lett.* **1993**, *75*, 2102−2105.

(39) Taleb, A.; Petit, C.; Pileni, M. P. Optical properties of self-assembled 2D and 3D superlattices of silver. *J. Phys. Chem*. **1998**, *B102*, 2214−2220 and references therein.
(40) Ohara, P. C.; Leff, D. V.; Heath, J. R.; Gelbart, W. M. Crystallization of opals from polydisperse nanoparticles. *Phys. Rev. Lett*. **1995**, *75*, 3466−69.
(41) Murray, C. B.; Kagan, C. R.; Bawendi, M. G. Self-organization of CdSe nanocrystallites into three-dimensional quantum dot superlattices. *Science* **1995**, *270*, 1335−1338.
(42) Bentzon, M. D.; Wonterghem, J. v.; Morup, S.; Tholen, A.; Koch, C. J. W. Ordered aggregates of ultrafine iron oxide particles: 'super crystals'. *Philos. Mag*. **1989**, *B60*, 169−178.
(43) Kiely, C. J.; Fink, J.; Brust, M.; Bethell, D.; Schiffrin, D. J. Spontaneous ordering of bimodal ensembles of nanoscopic gold clusters. *Nature* **1998**, *396*, 444−446.

AR970239T